Magazine of Civil Engineering. 2020. 95(3). Pp. 90–103

Magazine of Civil Engineering

ISSN 2071-0305

journal homepage: http://engstroy.spbstu.ru/

DOI: 10.18720/MCE.95.9

Method of plates stability analysis based on the moments approximations

Yu.Ya. Tyukalov*
Vyatka State University, Kirov, Russia
** E-mail: yutvgu@mail.ru*

Keywords: finite element method, plates, stability, approximations of forces, critical stress

Abstract. The paper proposes the method for calculating of thin plates stability by the finite element method based on piecewise constant approximations of the moments' fields. Using this approach may allow us to obtain the lower limit of critical stresses. We build the solution based on the extended functional of additional energy. The functional, using the method of Lagrange multipliers, includes algebraic equations of nodes equilibrium of the finite elements mesh. Using the possible displacements principle, we get equilibrium equations. The plate vertical displacements function after stability loss, is combination of linear basis functions. For rectangular and triangular finite elements there are the necessary expressions for the stresses work, acting in the plate median plane, from bending deformations. There are critical stress calculations for rectangular plates with different supporting conditions. The options for the action of compressive and shear stresses are considered. It is shown, that when the finite element mesh is refining up, the critical stress value in all the considered examples tends to the exact value from below. We perform comparison of the obtained solutions with the analytical solutions and the solutions by the program based on the finite element method in displacements. Comparison of solutions showed good accuracy in determining critical stresses by the proposed method.

1. Introduction

An analysis of elastic stability is necessary when we design many structural elements, especially thin plates. The study of the stability of elastic systems basically comes down to determining the magnitude of critical compressive loads which will lead to buckling of the structure. To ensure the margin of stability of structures, it is important to determine the lower limit of critical loads. The finite element method is one of the main methods for solving problems of stability theory, because it can be used to consider irregularities in constructions that cannot be allow in analytical methods [1, 2]. On the other hand, analytical methods using uniform approximations of displacements for the entire subject area make it possible to obtain more accurate and continuous solutions for plates with simple shapes [3, 4]. The solutions of stability problems for various structures by the finite element method in displacements are widely used [5, 6]. Such solutions are based on various functionals and use displacements fields approximations which may to allow the different deformations of structural elements [7, 8].

In [9], the solution of stability problem for spatial rod systems was obtained by the finite element method based on the forces approximations. This approach allowed to obtain the convergence of the critical load approximate value to exact value from below. To analyze the stability of the plates, the Ritz method is also often used [10–11]. Valid functions used to approximate displacements are a series of regular orthogonal polynomials which supplemented with special functions. The analysis performed in [11] shows the effectiveness and potential of the method which provides accurate results in combination with a reduced number of freedom degrees and simplified data preparation.

The stability analysis is great importance for the design of various steel plates [12–13]. In [13], the model was proposed for stability analysis of a corrugated steel plate. The proposed procedures only allow the linear elastic behavior of the material. The paper [14] is devoted to the analysis of the stability of variable thickness

This work is licensed under a CC BY-NC 4.0

plates. To modeling plate thickness variability, quadratic functions and the same nodal parameters are used, which approximate the displacements. To confirm the reliability of the proposed method, numerical results of stability plates calculations are presented. To analyze the stability of skew plates, a differential quadrature method was proposed in [15]. A complete set of equilibrium equations, in an inclined coordinate system, of bending and torques moments, equivalent transverse forces and angular forces is obtained. The accuracy of the solution was checked by comparing the results of inclined plates calculations, which had different boundary conditions, with the results obtained by the finite element method using very fine grids.

The use of analytical methods for solving the stability problems of plates is still relevant [16–17]. The main advantage of the analytical method is that it is simple and universal and does not require any predetermined deformations functions. In [17], the generalized integral transformation method was first used to obtain an exact analytical solution to the stability loss of a rectangular thin plate. In the article [18] it is given an idea of the implementation and using of the Ritz method for the analysis of free vibrations and loss of composite plates stability. Attention was paid to the selection of approximation functions depending on the degree and type of plates anisotropy. An efficient calculation method of Ritz integrals is proposed, which allows one to process a set of admissible functions. The effect of various forms of elastic bonds, boundary conditions and the material anisotropy variants on the convergence and accuracy of the solution was investigated. Various sets of admissible functions were used - Legendre and Chebyshev polynomials, as well as trigonometric type functions. The tasks of studying shallow shells stability [19] and plates of variable stiffness [20, 21] remain relevant. Alternative variational principles, in particular the Castilian's principle [22], are also used to solve various problems of elasticity theory. An important task is to study of plates stability during heating. In [23], experimental and theoretical studies of round plates during axisymmetric heating are presented.

In articles [24, 25], piecewise constant approximations of the moment fields were used to calculate bending plates by the finite element method. It was shown, that in this case when the finite element mesh is reducing the displacements values tend to exact values from above. This shows that the solution obtained using this technique is always more flexible than accurate. Thus, it can be assumed that the use of such approximations to analyze the stability of plates will allow us to obtain the lower boundary of the critical load.

The aim of this work is to develop a method for calculating the thin plates stability, which is based on piecewise constant approximations of the moment fields. The main tasks of paper are: obtaining the necessary resolving equations for rectangular and triangular finite elements; performing test calculations of critical forces for plates with different boundary conditions; comparison of the obtained solutions with analytical solutions and solutions obtained by programs which are based on the finite element method in displacements.

2. Methods

The solution to the stability problem of thin plates corresponding to Kirchhoff's theory will be built based on the additional energy functional [1]:

$$\Pi^c = \frac{1}{2}\frac{12}{E\cdot t^3}\int\limits_{\Omega}\left(M_x^2 + M_y^2 - 2\nu M_x M_y + 2\left(1+\nu\right)M_{xy}^2\right)\mathrm{d}\Omega. \tag{1}$$

E is the elastic modulus of the plate material; t is the plate thickness; ν is Poisson's ratio; M_x is bending moment directed along the X axis; M_y is bending moment directed along the Y axis; M_{xy} is torque. Bending moments are positive if they stretch the lower fibers of the plate. We write the functional (1) in matrix form:

$$\Pi^c = \frac{1}{2}\int\limits_{\Omega}\mathbf{M}_{\Omega}^{\mathrm{T}}\mathbf{E}^{-1}\mathbf{M}_{\Omega}\mathrm{d}\Omega. \tag{2}$$

The following notation is introduced in expression (2):

$$\mathbf{M}_{\Omega} = \begin{Bmatrix} M_x \\ M_y \\ M_{xy} \end{Bmatrix}, \quad \mathbf{E}^{-1} = \frac{12}{E\cdot t^3}\begin{bmatrix} 1 & -\nu & 0 \\ -\nu & 1 & 0 \\ 0 & 0 & 2\left(1+\nu\right) \end{bmatrix}. \tag{3}$$

We shall represent the subject area as a set of rectangular and triangular finite elements. In the region of the finite element for the moments fields we use piecewise constant approximation functions (Fig. 1) [24–26].

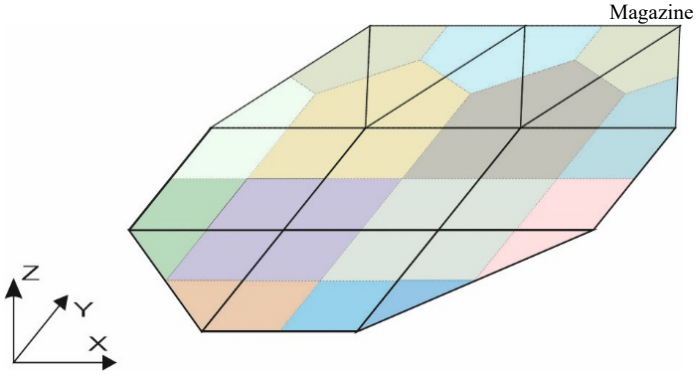

Figure 1. Piecewise constant approximations of the moments' fields. Areas with constant moments are shown in the same color.

We introduce the notation for unknown nodal moments $M_{x,i}, M_{\mathrm{y},i}, M_{xy,i}$ and for the vector of the nodal moments to the rectangular finite element

$$\mathbf{M}_k^{\mathrm{T}} = \left(M_{x,1} \quad M_{\mathrm{y},1} \quad M_{xy,1} \quad M_{x,2} \quad M_{\mathrm{y},2} \quad M_{xy,2} \quad M_{x,3} \quad M_{\mathrm{y},3} \quad M_{xy,3} \quad M_{x,4} \quad M_{\mathrm{y},4} \quad M_{xy,4} \right). \tag{4}$$

To simplify the notation of expressions, we introduce auxiliary unit stage functions

$$\psi_i(x,y) = \begin{cases} 1, & (x,y) \in \Omega_i \\ 0, & (x,y) \notin \Omega_i \end{cases}. \tag{5}$$

Also, we introduce the corresponding diagonal matrices which correspond to the element nodes

$$\boldsymbol{\Psi}_i = \begin{bmatrix} \psi_i & & \\ & \psi_i & \\ & & \psi_i \end{bmatrix}. \tag{6}$$

Then the approximation matrix of moments in the region of the rectangular finite element will have the simple form:

$$\mathbf{Z}_k = \begin{bmatrix} \boldsymbol{\Psi}_1 & \boldsymbol{\Psi}_2 & \boldsymbol{\Psi}_3 & \boldsymbol{\Psi}_4 \end{bmatrix}. \tag{7}$$

For a triangular finite element, expressions (4) and (7) are written similarly. Then

$$\mathbf{M}_\Omega = \mathbf{Z}_k \mathbf{M}_k. \tag{8}$$

Using (8), we shall express the additional strain energy of the finite element in the following form:

$$\Pi_k^c = \frac{1}{2} \int\limits_{\Omega_k} \mathbf{M}_k^{\mathrm{T}} \left(\mathbf{Z}_k^{\mathrm{T}} \mathbf{E}^{-1} \mathbf{Z}_k \right) \mathbf{M}_k \mathrm{d}\Omega. \tag{9}$$

We introduce the notation for the local flexibility matrix of the finite element $\mathbf{D}_k$:

$$\mathbf{D}_k = \int\limits_{\Omega_k} \mathbf{Z}_k^{\mathrm{T}} \mathbf{E}^{-1} \mathbf{Z}_k \mathrm{d}\Omega. \tag{10}$$

Note that the matrix is calculated analytically and has a block-diagonal form. Expressions of the matrix elements can be found in article [24].

From the flexibility matrices of finite elements $\mathbf{D}_k$, the global flexibility matrix of the construction $\mathbf{D}$ is formed, and from the vectors $\mathbf{M}_k$ global vector of nodal moments $\mathbf{M}$ is formed. Using the introduced notations, we obtain the following expression of the functional (2):

$$\Pi^c = \frac{1}{2} \mathbf{M}^{\mathrm{T}} \mathbf{D} \mathbf{M}. \tag{11}$$

It is important that the matrix $\mathbf{D}$ is block-diagonal and consists of square matrices measuring 3 by 3. Therefore, the matrix $\mathbf{D}$ is easily analytically reversible. This fact greatly simplifies construction of the problem solution.

In accordance with the Castigliano's principle, the moment fields must satisfy the equilibrium equations and static boundary conditions. To provide the equilibrium of the moment's fields, we compose the algebraic equilibrium equations of a grid nodes using the principle of possible displacements [24, 25].

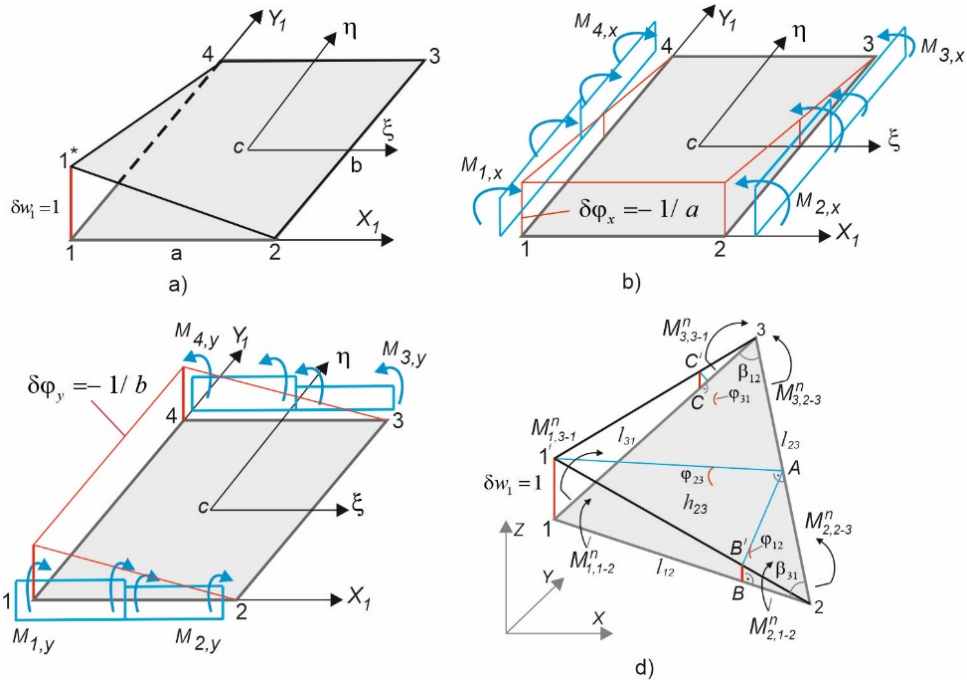

Figure 2. Possible of the node displacements:
a) possible of the node displacement for the rectangular element;
b) rotation angles of the sides which lie along the axis X_1;
c) rotation angles of the sides which lie along the axis Y_1;
d) possible displacements and rotation angles of the sides of the triangular element.

In Fig. 2 possible displacements of the node are shown. Linear functions are used to represent possible displacements at the finite element region. Therefore, the second derivatives of the possible displacements' functions will be equal to zero. Therefore, the moments which are normal to the finite element boundaries will be to do work on the corresponding rotation angles of the sides. But for a rectangular finite element, additional work will be performed by torques which will be constant over the element region.

Such equilibrium equations for finite element grid nodes are written as the system of linear homogeneous algebraic equations:

$$\mathbf{C}_i^{\mathrm{T}}\mathbf{M}_{i,eq} = 0, \quad i \in \Xi_z. \tag{12}$$

$\mathbf{M}_{i,eq}$ Is vector of nodal moments included in the equilibrium equation of node i. The equilibrium equation for a node will include unknown moments for nodes belonging to finite elements which are adjacent to node i. $\mathbf{C}_i$ is vector of coefficients at unknowns which are entering the equilibrium equation. In article [24] algorithm and necessary formulas for triangular and rectangular finite elements are presented.

When solving stability problems, at nodes, which are lying on some boundaries of the subject domain, the moment normal to the boundary (13) or the moment directed along boundary (14), or both, can be equal to zero.

$$M_{n,i} = M_{x,i}\cos^2\alpha_i + M_{y,i}\sin^2\alpha_i - 2M_{xy,i}\sin\alpha_i\cos\alpha_i = 0. \tag{13}$$

$$M_{ns,i} = \left(-M_{x,i} + M_{y,i}\right)\sin\alpha_i\cos\alpha_i + M_{xy,i}\left(\cos^2\alpha_i - \sin^2\alpha_i\right) = 0. \tag{14}$$

α_i is the angle between the tangent to the boundary at node i and the global axis X;

Using the Lagrange's multipliers method, we add the equilibrium equations (12) and the static boundary conditions (13–14) to the functional (11):

$$\Pi^c = \frac{1}{2}\mathbf{M}^{\mathrm{T}}\mathbf{D}\mathbf{M} + \sum_{i\in\Omega_z} w_i \mathbf{C}_i^{\mathrm{T}}\mathbf{M}_{i,eq} + \sum_{i\in\Omega_{\Gamma_n}} \varphi_{i,n} M_{n,i} + \sum_{i\in\Omega_{\Gamma_{ns}}} \varphi_{i,s} M_{ns,i}. \quad (15)$$

w_i Is displacement of the node i; $\varphi_{i,n}$, $\varphi_{i,s}$ are the Lagrange multipliers, which are additional nodal unknowns; Ω_z is set of nodes in which the vertical displacement is not equal to zero; Ω_{Γ_n}, $\Omega_{\Gamma_{ns}}$ is the sets of nodes which are lying on the boundary where the corresponding moments are equal to zero.

Expression (15) can be represented in the simpler matrix form:

$$\Pi^c = \frac{1}{2}\mathbf{M}^{\mathrm{T}}\mathbf{D}\mathbf{M} + \mathbf{w}^{\mathrm{T}}\mathbf{L}\mathbf{M}. \quad (16)$$

$\mathbf{L}$ is the "equilibrium" matrix of the whole system nodes. The number of this matrix rows is equal to the sum of number unknown nodal displacements and the number of static boundary conditions (13–14). The vector $\mathbf{w}$ includes unknown nodal displacements and Lagrange multipliers $\varphi_{i,n}$, $\varphi_{i,s}$.

To reduce the number of unknowns, one can use the penalty function method to include static boundary conditions. Then we get the following expression:

$$\Pi^c = \frac{1}{2}\mathbf{M}^{\mathrm{T}}\mathbf{D}\mathbf{M} + \mathbf{w}^{\mathrm{T}}\mathbf{L}\mathbf{M} + \alpha \sum_{i\in\Omega_{\Gamma_n}} M_{n,i}^2 + \alpha \sum_{i\in\Omega_{\Gamma_{ns}}} M_{ns,i}^2. \quad (17)$$

α is a large number, which is penalty parameter. In this case, the terms associated with the penalty functions are added to the elements of the matrix $\mathbf{D}$. Note that in this case, the matrix remains block-diagonal, and the expression of the functional takes the form (16).

If the boundary of the region is parallel to one of the global coordinate axes, then the static boundary conditions (13–14) can be allowed by excluding the corresponding unknown nodal moments. In further transformations, we will use for functional the expression (16).

As is known [1], when we solve the problem of plates stability it is necessary to consider additional tensile-compression deformities which are arising, when the plate is bending:

$$\varepsilon_{o,x} = \frac{1}{2}\left(\frac{\partial w}{\partial x}\right)^2, \varepsilon_{o,y} = \frac{1}{2}\left(\frac{\partial w}{\partial y}\right)^2, \varepsilon_{o,xy} = \frac{\partial w}{\partial x}\frac{\partial w}{\partial y}. \quad (18)$$

Deformations (18) correspond to the work of internal stresses $\sigma_x, \sigma_y, \sigma_{xy}$ acting in median plane of the plate. To obtain an expression of such work, we consider the rectangular finite element (Fig. 1). The vertical displacements of the plate, when one loss of stability, are represented by linear basis functions:

$$w(x,y) = \sum_{i=1}^{4} \frac{(1+\xi\xi_i)(1+\eta\eta_i)}{4}\overline{w}_i, \xi = \frac{2x}{a}, \eta = \frac{2y}{b}. \quad (19)$$

$\overline{w}_i$ is displacement of node i. Then we obtain the following expressions for derivatives included in expressions (18):

$$\frac{\partial w}{\partial x} = \sum_{i=1}^{4} \frac{\xi_i(1+\eta\eta_i)}{2a}\overline{w}_i, \frac{\partial w}{\partial y} = \sum_{i=1}^{4} \frac{\eta_i(1+\xi\xi_i)}{2b}\overline{w}_i. \quad (20)$$

The work of stresses $\sigma_x, \sigma_y, \sigma_{xy}$ is expressed by the integral over the finite element area

$$U_{\varepsilon_o}^* = \int_0^a \int_0^b t(\sigma_x\varepsilon_{o,x} + \sigma_y\varepsilon_{o,y} + \sigma_{xy}\varepsilon_{o,xy})dxdy. \quad (21)$$

In further transformations we will use the vector of unknown nodal displacements $\mathbf{w}_k$ and the vectors $\mathbf{N}_{k,x}$, $\mathbf{N}_{k,y}$ for finite element with index k:

$$\mathbf{w}_k = \begin{Bmatrix} \overline{\mathrm{w}}_1 \\ \overline{\mathrm{w}}_2 \\ \overline{\mathrm{w}}_3 \\ \overline{\mathrm{w}}_4 \end{Bmatrix}, \mathbf{N}_{k,x} = \begin{Bmatrix} \frac{\xi_1(1+\eta\eta_1)}{2a} \\ \frac{\xi_2(1+\eta\eta_2)}{2a} \\ \frac{\xi_3(1+\eta\eta_3)}{2a} \\ \frac{\xi_4(1+\eta\eta_4)}{2a} \end{Bmatrix}, \mathbf{N}_{k,y} = \begin{Bmatrix} \frac{\eta_1(1+\xi\xi_1)}{2b} \\ \frac{\eta_2(1+\xi\xi_2)}{2b} \\ \frac{\eta_3(1+\xi\xi_3)}{2b} \\ \frac{\eta_4(1+\xi\xi_4)}{2b} \end{Bmatrix}. \tag{22}$$

Using (22) we obtain the following matrix expressions for strains (18):

$$\varepsilon_{o,x} = \frac{1}{2}\mathbf{w}_k^{\mathrm{T}}\left(\mathbf{N}_{k,x}\mathbf{N}_{k,x}^{\mathrm{T}}\right)\mathbf{w}_k, \quad \varepsilon_{o,y} = \frac{1}{2}\mathbf{w}_k^{\mathrm{T}}\left(\mathbf{N}_{k,\mathrm{y}}\mathbf{N}_{k,\mathrm{y}}^{\mathrm{T}}\right)\mathbf{w}_k, \quad \varepsilon_{o,xy} = \mathbf{w}_k^{\mathrm{T}}\left(\mathbf{N}_{k,\mathrm{x}}\mathbf{N}_{k,\mathrm{y}}^{\mathrm{T}}\right)\mathbf{w}_k. \tag{23}$$

Next, we obtain the expression for the work of stresses $\sigma_x, \sigma_y, \sigma_{xy}$:

$$U_{\varepsilon_o}^{*} = \frac{ab}{4}\int_{-1}^{1}\int_{-1}^{1} t\left(\frac{1}{2}\sigma_x\mathbf{w}_k^{\mathrm{T}}\left(\mathbf{N}_{k,x}\mathbf{N}_{k,x}^{\mathrm{T}}\right)\mathbf{w}_k + \frac{1}{2}\sigma_y\mathbf{w}_k^{\mathrm{T}}\left(\mathbf{N}_{k,y}\mathbf{N}_{k,y}^{\mathrm{T}}\right)\mathbf{w}_k + \sigma_{xy}\mathbf{w}_k^{\mathrm{T}}\left(\mathbf{N}_{k,\mathrm{x}}\mathbf{N}_{k,y}^{\mathrm{T}}\right)\mathbf{w}_k\right)\mathrm{d}\xi\,\mathrm{d}\eta. \tag{24}$$

To simplify we introduce the notation for the following matrices:

$$\begin{gathered} \mathbf{H}_{k,x} = \frac{abt}{4}\int_{-1}^{1}\int_{-1}^{1}\sigma_x\mathbf{N}_{k,x}\mathbf{N}_{k,x}^{\mathrm{T}}\,\mathrm{d}\xi\,\mathrm{d}\eta,\ \mathbf{H}_{k,y} = \frac{abt}{4}\int_{-1}^{1}\int_{-1}^{1}\sigma_y\mathbf{N}_{k,\mathrm{y}}\mathbf{N}_{k,\mathrm{y}}^{\mathrm{T}}\,\mathrm{d}\xi\,\mathrm{d}\eta, \\ \mathbf{H}_{k,xy} = \frac{abt}{4}\int_{-1}^{1}\int_{-1}^{1}\sigma_{xy}\mathbf{N}_{k,x}\mathbf{N}_{k,y}^{\mathrm{T}}\,\mathrm{d}\xi\,\mathrm{d}\eta. \end{gathered} \tag{25}$$

After integration, we obtain the following expressions for matrix elements:

$$\mathbf{H}_{k,x} = \frac{\sigma_x bt}{6a}\begin{bmatrix} 2 & -2 & -1 & 1 \\ -2 & 2 & 1 & -1 \\ -1 & 1 & 2 & -2 \\ 1 & -1 & -2 & 2 \end{bmatrix}, \mathbf{H}_{k,y} = \frac{\sigma_y at}{6b}\begin{bmatrix} 2 & 1 & -1 & -2 \\ 1 & 2 & -2 & -1 \\ -1 & -2 & 2 & 1 \\ -2 & -1 & 1 & 2 \end{bmatrix}, \mathbf{H}_{k,xy} = \frac{\sigma_{xy}t}{4}\begin{bmatrix} 1 & 1 & -1 & -1 \\ -1 & -1 & 1 & 1 \\ -1 & -1 & 1 & 1 \\ 1 & 1 & -1 & -1 \end{bmatrix}. \tag{26}$$

$$U_{\varepsilon_o}^{*} = \frac{1}{2}\mathbf{w}_k^{T}\left(\mathbf{H}_{k,x} + \mathbf{H}_{k,y}\right)\mathbf{w}_k + \mathbf{w}_k^{T}\mathbf{H}_{k,xy}\mathbf{w}_k. \tag{27}$$

Calculating the derivative of additional energy, we obtain:

$$\mathbf{H}_k = \frac{\mathrm{d}U_{\varepsilon_o}^{*}}{\mathrm{d}\mathbf{w}_k} = \left(\mathbf{H}_{k,x} + \mathbf{H}_{k,y} + \mathbf{H}'_{k,xy}\right)\mathbf{w}_k, \quad \mathbf{H}'_{k,xy} = \frac{\sigma_{xy}t}{2}\begin{bmatrix} 1 & 0 & -1 & 0 \\ 0 & -1 & 0 & 1 \\ -1 & 0 & 1 & 0 \\ 0 & 1 & 0 & -1 \end{bmatrix}. \tag{28}$$

From geometric matrices of finite elements $\mathbf{H}_k$, the global geometric matrix $\mathbf{H}$ is formed for entire system, and from vectors $\mathbf{w}_k$ is formed the global vector of nodal displacements $\mathbf{w}$.

Using the notation introduced, we obtain the matrix expression for the work of internal stresses acting in the plate middle plane

$$U_{\varepsilon_o}^{*} = \frac{1}{2}\mathbf{w}^{\mathrm{T}}\mathbf{H}\mathbf{w}. \tag{29}$$

Next, we obtain expressions of geometric matrices for a triangular finite element. The vertical displacement function for the triangular finite element of the plate is represented using the triangular coordinates:

$$w(x,y)=\sum_{i=1}^{3}L_i(x,y)\overline{w}_i,\ L_i(x,y)=\frac{1}{2A}(a_i+b_ix+c_iy),$$
$$a_i=x_{i+1}y_{i+2}-x_{i+2}y_{i+1},\ b_i=y_{i+1}-y_{i+2},\ c_i=x_{i+2}-x_{i+1}. \tag{30}$$

x_i, y_i is coordinates of the nodes of the finite element in the global coordinate system; $\overline{w}_i$ is vertical displacement of the node; A is area of the finite element. The partial derivatives of the displacement functions (30) will be constant functions:

$$\frac{\partial w}{\partial x}=\frac{1}{2A}\sum_{i=1}^{3}b_i\overline{w}_i,\ \frac{\partial w}{\partial y}=\frac{1}{2A}\sum_{i=1}^{3}c_i\overline{w}_i. \tag{31}$$

Vectors like (22) will have the following view:

$$\mathbf{w}_k=\begin{Bmatrix}\overline{\mathrm{w}}_1\\ \overline{\mathrm{w}}_2\\ \overline{\mathrm{w}}_3\end{Bmatrix},\quad \mathbf{N}_{k,x}=\frac{1}{A}\begin{Bmatrix}b_1\\ b_2\\ b_3\end{Bmatrix},\quad \mathbf{N}_{k,\mathrm{y}}=\frac{1}{A}\begin{Bmatrix}c_1\\ c_2\\ c_3\end{Bmatrix}. \tag{32}$$

The stresses work in this case is calculated as an integral over the triangle area:

$$U_{\varepsilon_o}^{*}=\int_A t(\sigma_x\varepsilon_{o,x}+\sigma_y\varepsilon_{o,y}+\sigma_{xy}\varepsilon_{o,xy})dA. \tag{33}$$

Substituting expressions for deformations (18) in (33), we obtain expressions for the geometric matrices' elements of the triangular finite element (which are like the matrices (25)):

$$\mathbf{H}_{k,x}=\frac{\sigma_x t}{4A}\begin{bmatrix}b_1^2 & b_1b_2 & b_1b_3\\ b_1b_2 & b_2^2 & b_2b_3\\ b_1b_3 & b_2b_3 & b_3^2\end{bmatrix},\mathbf{H}_{k,y}=\frac{\sigma_y t}{4A}\begin{bmatrix}c_1^2 & c_1c_2 & c_1c_3\\ c_1c_2 & c_2^2 & c_2c_3\\ c_1c_3 & c_2c_3 & c_3^2\end{bmatrix},\mathbf{H}_{k,xy}=\frac{\sigma_{xy} t}{4A}\begin{bmatrix}b_1c_1 & b_1c_2 & b_1c_3\\ b_2c_1 & b_2c_2 & b_2c_3\\ b_3c_1 & b_3c_2 & b_3c_3\end{bmatrix}. \tag{34}$$

Calculating the derivative of additional energy $U_{\varepsilon_o}^{*}$, we obtain:

$$\mathbf{H}_k=\frac{\mathrm{d}U_{\varepsilon_o}^{*}}{\mathrm{d}\mathbf{w}_k}=\left(\mathbf{H}_{k,x}+\mathbf{H}_{k,y}+\mathbf{H}'_{k,xy}\right)\mathbf{w}_k,\mathbf{H}'_{k,xy}=\frac{\sigma_{xy} t}{4A}\begin{bmatrix}2b_1c_1 & b_1c_2+b_2c_1 & b_1c_3+b_3c_1\\ b_1c_2+b_2c_1 & 2b_2c_2 & b_2c_3+b_3c_2\\ b_1c_3+b_3c_1 & b_2c_3+b_3c_2 & 2b_3c_3\end{bmatrix}. \tag{35}$$

Thus, to solve the stability problems of Kirchhoff plates, it is necessary to add to the functional (16) the work of internal stresses acting in the middle plane which is multiplied by the critical load parameter λ_{cr}. Summing up (16) and (29), we obtain the following functional for solving the plate stability problem:

$$\Pi^c=\frac{1}{2}\mathbf{M}^{\mathrm{T}}\mathbf{D}\mathbf{M}+\mathbf{w}^{\mathrm{T}}\mathbf{L}\mathbf{M}+\frac{\lambda_{cr}}{2}\mathbf{w}^{\mathrm{T}}\mathbf{H}\mathbf{w}. \tag{36}$$

To obtain solving equations, we equate to zero derivatives (36) with respect to the vectors $\mathbf{M}$ and $\mathbf{w}$:

$$\mathbf{D}\mathbf{M}+\mathbf{L}^T\mathbf{w}=0,$$
$$\mathbf{L}\mathbf{M}+\lambda_{cr}\mathbf{H}\mathbf{w}=0. \tag{37}$$

Expressing the vector from the first equation and substituting it into the second equation, we obtain:

$$\mathbf{L}\mathbf{D}^{-1}\mathbf{L}^T\mathbf{w}-\lambda_{cr}\mathbf{H}\mathbf{w}=0. \tag{38}$$

We introduce the notation for the product of matrices:

$$\mathbf{K}=\mathbf{L}\mathbf{D}^{-1}\mathbf{L}^T. \tag{39}$$

Using (39), we obtain the algebraic equations system for determining the critical parameter λ_{cr}:

$$\mathbf{K}\mathbf{w}=\lambda_{cr}\mathbf{H}\mathbf{w}. \tag{40}$$

As noted above, the matrix $\mathbf{D}$ is block-diagonal form and is easily reversible analytically. The matrix $\mathbf{D}^{-1}$ will also is block-diagonal form, therefore, the matrix $\mathbf{K}$ is a tape structure of nonzero elements, which significantly reduces the computational cost of solving the equations system. To calculate the elements of the matrix $\mathbf{K}$, you can use special algorithm to reduce the computational operations number for its formation.

To determine the critical value of the parameter, we apply the well-known reverse iterations method, which includes the following steps:

$$\begin{cases} \text{set the vector } \mathbf{w}_0,\ i=0; \\ \text{cycle } i=i+1; \\ \mathbf{K}\mathbf{w}_i=\mathbf{H}\mathbf{w}_{i-1}; \\ w_{\max}=\max\left|w_{i,j}\right|,\ j=1..n; \\ \lambda_{cr,i}=\dfrac{1}{w_{\max}}; \\ \mathbf{w}_i=\dfrac{1}{w_{\max}}\mathbf{w}_i; \\ \mathbf{w}_i=\dfrac{\mathbf{w}_i+\mathbf{w}_{i-1}}{2}; \\ \text{cycle end, if } \dfrac{\left|\lambda_{cr,i}-\lambda_{cr,i-1}\right|}{\lambda_{cr,i}}\le\varepsilon. \end{cases} \tag{41}$$

In (41), $w_{\max}$ is the maximum element of the nodal displacements vector $\mathbf{w}_i$ by modulus. Parameter ε determines the calculation accuracy of the critical parameter.

3. Results and Discussion

In [27], analytical solutions are given for the Kirchhoff plates stability problems with different supporting conditions. For comparison with analytical solutions, calculations were carried out to determine the critical stresses σ_x for the hinged plates shown in Fig. 3. The calculations were performed for grids consisting of rectangular and triangular finite elements (see Fig. 3).

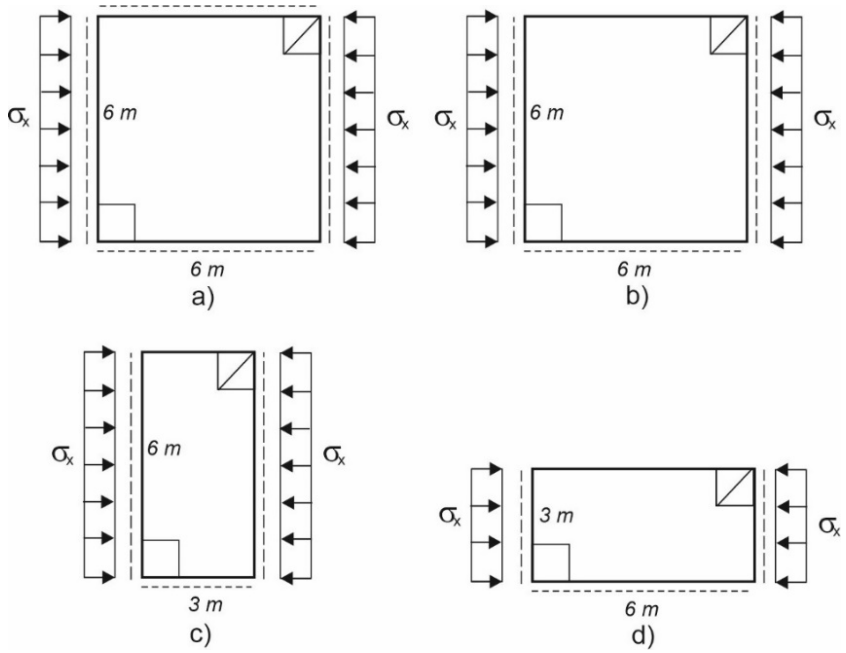

Figure 3. Hinged plates under the action of compressive load along the X axis: a) square hinged-supported plate on all sides; b) square plate hinged-supported on three sides; c) rectangular plate hinged-supported on three sides and the short side is free; d) a rectangular plate hinged-supported on three sides and the long side is free.

In the calculations, the following parameters were taken for the plate: $t = 1m, E = 10\,kN/m^2, \mu = 0.3$. The hinged-supported sides of the plates are indicated by dashed line in Fig. 3. In the nodes, lying on the hinged-supported sides, moments directed perpendicular to this side were taken zero. In the nodes lying on the free side, also torques were taken zero. Tables 1–4 show the critical stress values σ_x calculated by the proposed methodology (SFEM), using the LIRA-SAPR program and obtained analytically [27].

Table 1. The critical stress $\sigma_x, kN/m^2$ for the plate in Fig. 3a.

Grid	SFEM		LIRA-SAPR	
	□	◺	□	◺
10x10	0.97938	0.99845	0.99373	1.01433
20x20	0.99796	1.00270	1.00157	1.00675
30x30	1.00144	1.00353	1.00305	1.00535
40x40	1.00266	1.00383	1.00357	1.00487
[27]	1.00423			

Table 2. The critical stress $\sigma_x, kN/m^2$ for the plate in Fig. 3b.

Grid	SFEM		LIRA-SAPR	
	□	◺	□	◺
10x10	0.33991	0.33376	0.35202	0.35360
20x20	0.34703	0.34898	0.35193	0.35231
30x30	0.34890	0.35365	0.35190	0.35207
40x40	0.34975	0.35582	0.35189	0.35199
[27]	0.361525			

Table 3. The critical stress $\sigma_x, kN/m^2$ for the plate in Fig. 3c.

Grid	SFEM		LIRA-SAPR	
	□	◺	□	◺
5x10	1.06470	1.06311	1.09547	1.10081
10x20	1.08211	1.08490	1.09432	1.09538
15x30	1.08660	1.09150	1.09392	1.09436
20x40	1.08859	1.09457	1.09376	1.09404
[27]	1.10465			

Table 4. The critical stress $\sigma_x, kN/m^2$ for the plate in Fig. 3d.

Grid	SFEM		LIRA-SAPR	
	□	◺	□	◺
10x5	1.17417	1.11743	1.33114	1.37259
20x10	1.27265	1.26725	1.33916	1.34975
30x15	1.29980	1.30917	1.34055	1.34504
40x20	1.31193	1.32751	1.34103	1.34259
[27]	1.38584			

In Fig. 4, the data from Tables 1–4 are presented in the form of graphs of the critical compression stress value. The divisions number of the plates long side is shown at the horizontal axis. The divisions number of the short side was half as much.

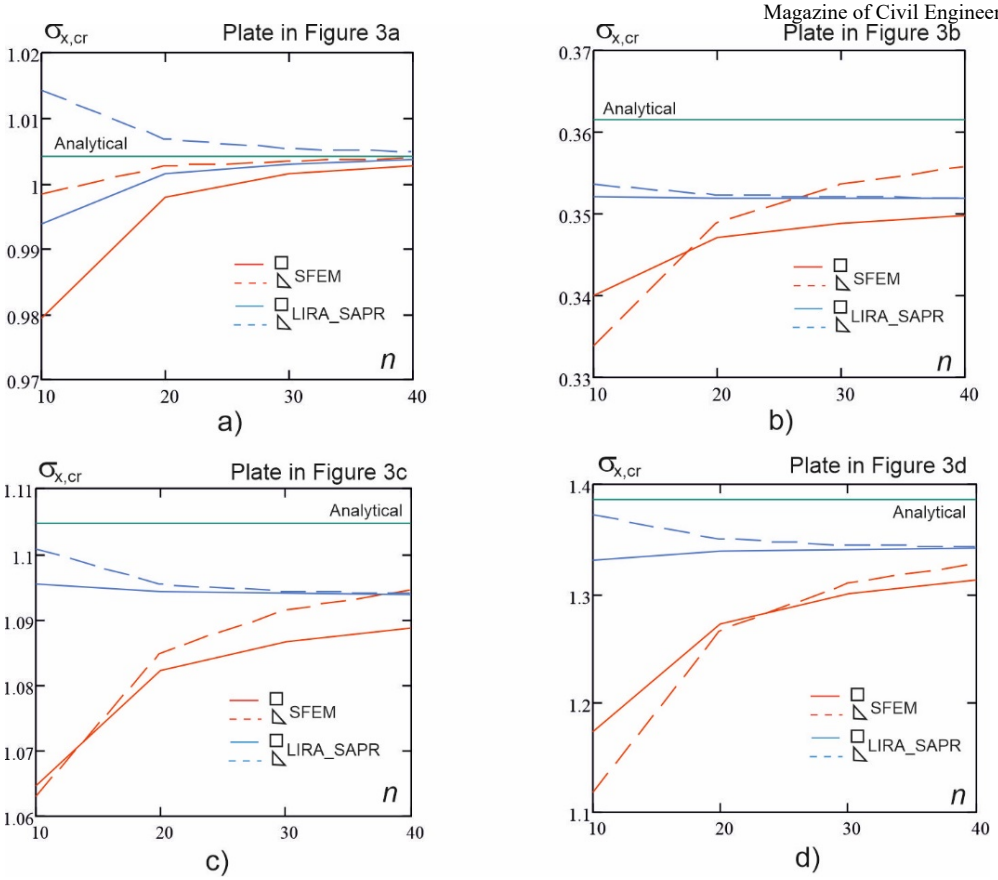

Figure 4. Graphs of the critical stress dependence on the divisions number of the plates long side, which are shown in Figure 3. Red lines are solutions obtained by the proposed SFEM method. Blue lines are LIRA-SAPR solutions. Solid lines are solutions obtained for the grid of rectangular elements. Dotted lines are solutions obtained for the grid of triangular elements. Green lines are analytical solutions [27].

The results show that the critical stresses calculated by the proposed method, when grinding up the finite elements mesh, tend to exact values from below. Thus, the proposed calculation method, based on piecewise constant approximations of the moment functions, provides the lower boundary of critical compressive stresses for the consideration plates. Such results are expected, since it was shown in [24, 25] that, using such approximations to calculate bending plates, we obtain convergence of displacements values to exact magnitudes from above. The proposed finite element model reduces the plate flexural rigidity, compared with the real rigidity, so we get lower values of critical compressive stresses. We also note that for the smallest grids, the critical stresses obtained based on the stress approximation for three plate options are closer to the analytical solutions that the solutions using the LIRA-SAPR program. Only for the plate in Fig. 3d the solution obtained by the LIRA-SAPR program is closer to the analytical one. But at the same time, when mesh grinding up the critical stress decreases and the solution moves away from the analytical one (Table 4).

Also, calculations were carried out to determine the critical stresses for plates in which one side is pinched (Fig. 5). The material characteristics were taken to be the same as in the previous example.

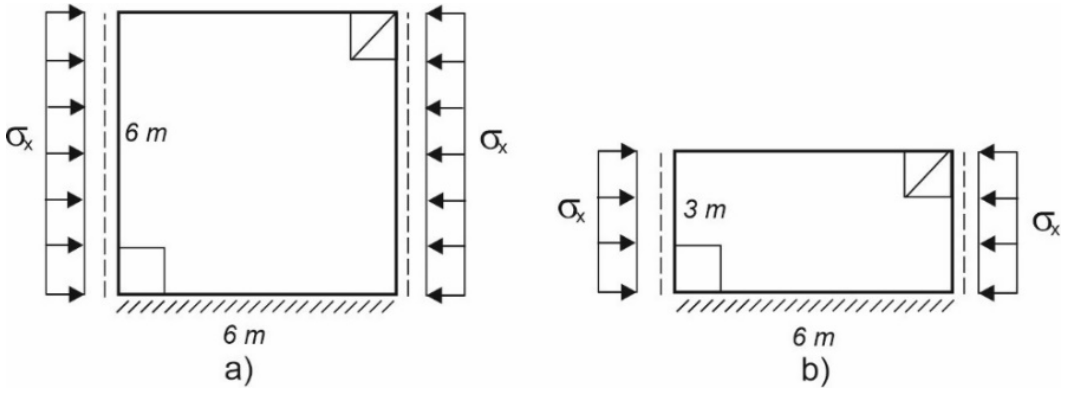

Figure 5. Plates with two hinged support sides and with one pinched side and one free.

Table 5. The critical stress $\sigma_x, kN/m^2$ for the plate in Fig. 5a.

Grid	SFEM		LIRA-SAPR	
	□	◺	□	◺
10x10	0.39418	0.39879	0.41440	0.41720
20x20	0.40658	0.41798	0.41477	0.41543
30x30	0.40986	0.42321	0.41483	0.41512
40x40	0.41131	0.42545	0.41485	0.41501
[27]	0.42680			

Table 6. The critical stress $\sigma_x, kN/m^2$ for the plate in Fig. 5b.

Grid	SFEM		LIRA-SAPR	
	□	◺	□	◺
10x10	1.17417	1.11745	1.33114	1.37259
20x20	1.27265	1.26725	1.33916	1.34975
30x30	1.29980	1.30917	1.34055	1.34504
40x40	1.31195	1.32757	1.34103	1.34259
[27]	1.38584			

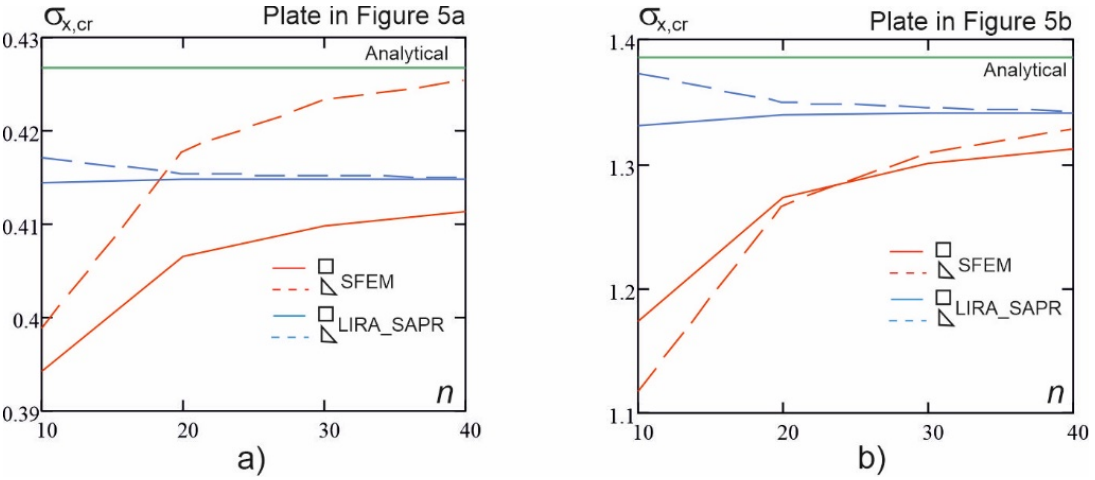

Figure 6. Graphs of the critical stress dependencies on the plate long side divisions number (Figure 5).

The calculation results for the plate with pinched side (Fig. 5) confirm the conclusions which made at discussing the previous example results. The critical stress values obtained by the proposed method (SFEM), when grinding up the finite element mesh, approach the analytical solution from below. This direction of solution convergence provides the critical stress lower boundary. Note that in the proposed method for the displacement approximations in the finite element region, after loss of stability, simple linear functions are used. Therefore, with coarse grids, the critical forces values are calculated with a larger error, compared with the values obtained using the LIRA-SAPR program which uses displacements approximations a higher order. But, as the calculation results show, when we solve using the LIRA-SAPR program which is based on the displacements approximations we do not have a certain direction of approximate solution convergence to the exact one. In some cases, when the mesh of finite elements is refined up, the value of the critical force increases, but in many cases, it decreases (see blue lines in Fig. 4 and Fig. 6).

Also, stability calculations of hinged-supported plates by the tangent stresses action were performed (Fig. 7). The square plate (Fig. 7a) and the plate with one to two aspect ratios (Fig. 7b) were calculated. For the subject area discretization rectangular and triangular grids of finite elements were used. Calculation results comparison with the analytical solutions [27] is presented in Table 7–8 and in Fig. 8.

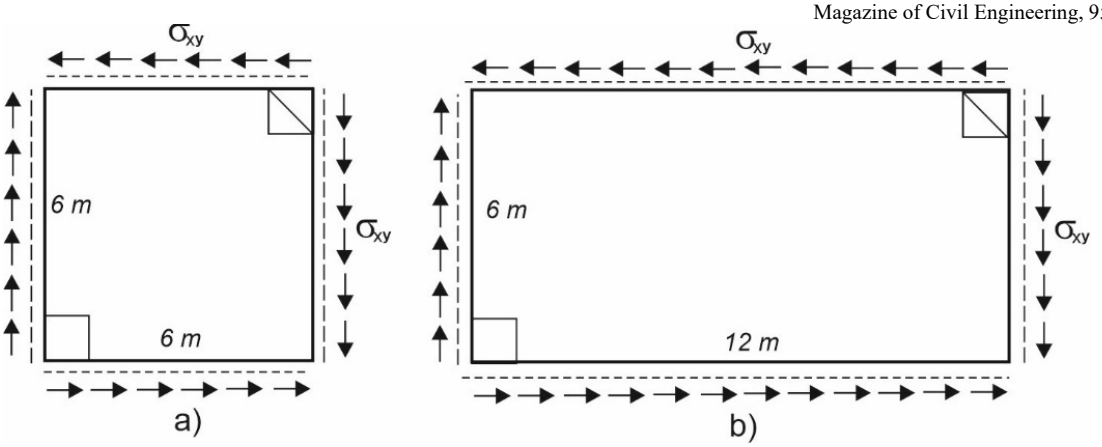

Figure 7. Hinged-supported plates. The action of tangent stresses.

Table 7. The critical stresses $\sigma_{xy}, kN/m^2$ for the plate in Fig. 7a.

Grid	SFEM		LIRA-SAPR	
	□	◺	□	◺
10x10	2.23904	2.24885	2.27247	2.38643
20x20	2.22525	2.31822	2.32265	2.35250
30x30	2.33737	2.33081	2.33273	2.34610
40x40	2.34287	2.34045	2.35057	2.34368
[27]	2.36497			

Table 8. The critical stresses $\sigma_{xy}, kN/m^2$ for the plate in Fig. 7b.

Grid	SFEM		LIRA-SAPR	
	□	◺	□	◺
10x6	1.50975	1.56137	1.55895	1.69831
20x12	1.62150	1.63299	1.62299	1.65734
30x16	1.64095	1.64727	1.63322	1.65022
40x40	1.64921	1.65315	1.63753	1.64754
[27]	1.65698			

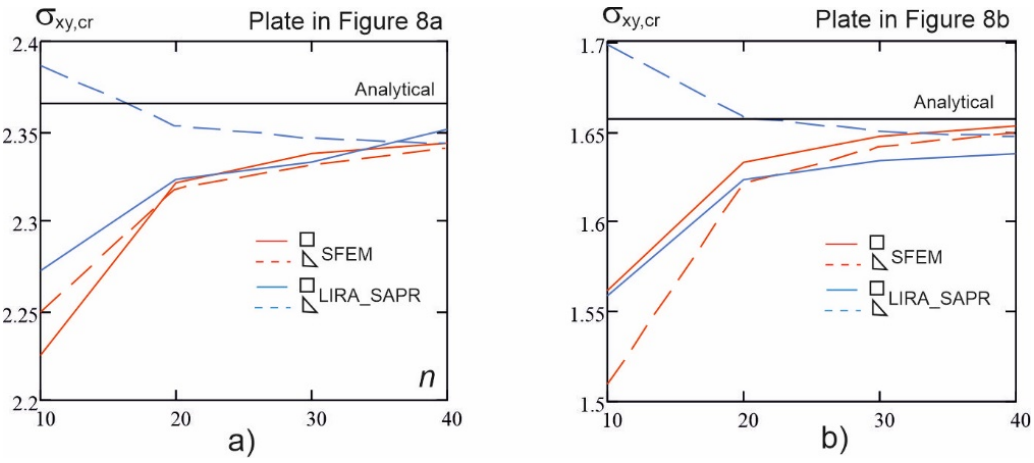

Figure 8. The critical stresses dependence graphs on the number of the long sides divisions of the shown in Figure 7 plates.

The graphs in Fig. 8 shows that the critical tangent stresses values obtained based on the stress approximation (SFEM) tend to analytical values from below when the finite element mesh is refined up. The critical tangent stresses which obtained using the LIRA-SAPR program for the triangular finite elements decrease when mesh is refined up. Thus, approximate solutions which are obtained based on the displacement approximations can converge to the exact solution from different sides.

4. Conclusion

1. The stability analysis method of thin plates, which is based on piecewise constant approximations of the moments, is proposed. The solution is based on the additional energy functional. For the finite element grid nodes, using the principle of possible displacements, algebraic equilibrium equations are formed, which are then added to the functional of additional energy by using Lagrange multipliers.

2. To calculate the work of the stresses acting in the plate median plane, the plate vertical displacements function after stability loss, is represented by linear basis functions. The necessary solving relations for rectangular and triangular finite elements are obtained.

3. According to the proposed method, critical stress calculations were performed for rectangular plates with different supporting conditions. The options for the action of compressive and shear stresses are considered. It is shown, that when the finite element mesh is refining up, the critical stress value in all the considered examples tends to the exact value from below. That direction of the solution convergence provides the lower boundary of the critical stress value.

4. The obtained solutions are compared with the analytical solutions and the solutions obtained by the LIRA-SAPR program. The solutions comparison showed good accuracy in determining critical stresses which are calculated by the proposed method.

References

1. Gallagher, R.H. Finite Element Analysis: Fundamentals. Englewood Cliffs, Prentice-Hall, 1975. 420 p.
2. Eslami, M.R. Buckling and Postbuckling of Beams, Plates and Shells. New York: Springer, 2018. 588 p.
3. Sukhoterin, M.V., Baryshnikov, S.O., Knysh, T.P., Abdikarimov, R.A. Natural oscillations of a rectangular plates with two adjacent edges clamped // Magazine of Civil Engineering. 2018. No. 6(82). Pp. 81–94. DOI: 10.18720/MCE.82.8
4. Mirsaidov, M.M., Abdikarimov, R.A., Vatin, N.I., Zhgutov, V.M., Khodzhayev, D.A., Normuminov, B.A. Nonlinear parametric oscillations of viscoelastic plate of variable thickness // Magazine of Civil Engineering. 2018. No. 6(82). Pp. 112–126. DOI: 10.18720/MCE.82.11
5. Rybakov, V.A., Lalin, V.V., Ivanov, S.S., Azarov, A.A. Coordinate functions quadratic approximation in V.I. Slivker's semi-shear stability theory // Magazine of Civil Engineering. 2019. No. 5(89). Pp. 115–128. DOI: 10.18720/MCE.89.10
6. Le, T., Lalin, V.V., Bratashov, A.A. Static accounting of highest modes in problems of structural dynamics // Magazine of Civil Engineering. 2019. No. 4(88). Pp. 3–13. DOI: 10.18720/MCE.88.1
7. Lalin, V.V., Rybakov, V.A., Dyakov, S.F., Kudinov, V.V., Orlova, Ye.S. The semi-shear theory of V.I. Slivker for the stability problems of thin-walled bars // Magazine of Civil Engineering. 2019. No. 3(87). Pp. 66–79. DOI: 10.18720/MCE.87.6
8. Tyukalov, Yu.Ya. Refined finite element of rods for stability calculation // Magazine of Civil Engineering. 2018. No. 3(79). Pp. 54–65. DOI: 10.18720/MCE.79.6
9. Tyukalov, Yu.Ya. The functional of additional energy for stability analysis of spatial rod systems // Magazine of Civil Engineering. 2017. No. 2(70). Pp. 18–32. DOI: 10.18720/MCE.70.3
10. Chen, D., Yang, J., Kitipornchai, S. Buckling and bending analyses of a novel functionally graded porous plate using Chebyshev-Ritz method. Archives of Civil and Mechanical Engineering. 2019. Vol. 19. Pp. 157–170.
11. Milazzo, A., Benedetti, I., Gulizzi, V. A single-domain Ritz approach for buckling and post-buckling analysis of cracked plates. International Journal of Solids and Structures. 2019. Vol. 159. Pp. 221–231.
12. Vu, Q.-V., Truong, V.-H., Papazafeiropoulos, G., Graciano, C., Kim, S.-E. Bend-buckling strength of steel plates with multiple longitudinal stiffeners. Journal of Constructional Steel Research. 2019. Vol. 158. Pp. 41–52.
13. Gajdzicki, M., Perliński, W., Michalak, B. Stability analysis of bi-directionally corrugated steel plates with orthotropic plate model. Engineering Structures. 2018. Vol. 160. Pp. 519–534.
14. Le-Manh, T., Huynh-Van, Q., Phan, T., Phan, H., Nguyen-Xuan, H. Isogeometric nonlinear bending and buckling analysis of variable-thickness composite plate structures. Composite Structures. 2017. Vol. 159. Pp. 818–826.
15. Wang, X., Yuan, Z. Buckling analysis of isotropic skew plates under general in-plane loads by the modified differential quadrature method. Applied Mathematical Modelling. 2018. Vol. 56. Pp. 83–95.
16. Li, S., Hu, Z., Benson, S. An analytical method to predict the buckling and collapse behaviour of plates and stiffened panels under cyclic loading. Engineering Structures. 2019. Vol. 199. Article 109627.
17. Ullah, S., Zhong, Y., Zhang, J. Analytical buckling solutions of rectangular thin plates by straightforward generalized integral transform method. International Journal of Mechanical Sciences. 2019. Vol. 152. Pp. 535–544.
18. Vescovini, R., Dozio, L., D'Ottavio, M., Polit, O. On the application of the Ritz method to free vibration and buckling analysis of highly anisotropic plates. Composite Structures. 2018. Vol. 192. Pp. 460–474.
19. Kamenev, I.V., Semenov, A.A. Ustoychivost pologikh ortotropnykh obolochek dvoyakoy krivizny pri sharnirno-podvizhnom zakreplenii kontura [Stability of shallow orthotropic shells of double curvature during articulated-movable fastening of the contour] // Vestnik Permskogo natsionalnogo issledovatelskogo politekhnicheskogo universiteta. Mekhanika. 2018. No. 2. Pp. 32–43. (rus) DOI: 10.15593/perm.mech/2018.2.04
20. Abdikarimov, R.A., Khudayarov, B. Dynamic stability of viscoelastic flexible plates of variable stiffness under axial compression. International Applied Mechanics. 2014. Vol. 50. Pp. 389–398.
21. Abdikarimov, R., Khudayarov, B. Vatin, N.I. To Calculation of Rectangular Plates on Periodic Oscillations. MATEC Web of Conferences. 2018. Vol. 245. 01003.

22. Kuznetsova, Y.S., Vorobyev, N.A., Trufanov, N.A. Application of the geometric immersion method based on the castigliano variational principle for the axisymmetric problems of elasticity theory. IOP Conference Series: Materials Science and Engineering. 2017. Pp. 012125.
23. Goldshteyn, R.V., Popov, A.L., Kozintsev, V.M., Chelyubeyev, D.A. Neosesimmetrichnaya poterya ustoychivosti pri osesimmetrichnom nagreve krugloy plastiny [Axisymmetric buckling during axisymmetric heating of a round plate] // Vestnik Permskogo natsionalnogo issledovatelskogo politekhnicheskogo universiteta. Mekhanika. 2016. No. 2. Pp. 45–53. (rus) DOI: 10.15593/perm.mech/2016.2.04
24. Tyukalov, Yu.Ya. Finite element models in stresses for bending plates // Magazine of Civil Engineering. 2018. No. 6(82). Pp. 170–190. DOI: 10.18720/MCE.82.16
25. Tyukalov, Yu.Ya. Calculation method of bending plates with assuming shear deformations // Magazine of Civil Engineering. 2019. No. 1(85). Pp. 107–122. DOI: 10.18720/MCE.85.9
26. Tyukalov, Yu.Ya. Finite element models in stresses for plane elasticity problems // Magazine of Civil Engineering. 2018. No. 1(77). Pp. 23–37. DOI: 10.18720/MCE.77.3
27. Timoshenko, S.P. Ustoychivost sterzhney, plastin i obolochek [Stability of rods, plates and shells]. Moskow: Nauka, 1971. 808 p. (rus)

Contacts:

Yury Tyukalov, yutvgu@mail.ru

© Tyukalov Yu.Ya., 2020